Variation of small strain shear properties of loose sand induced by liquefaction
（液状化によるゆるい砂の微小せん断特性の変化）

Muhammad Rizwan
Professor: Hirofumi Toyota

ABSTRACT

Liquefaction significantly affects the mechanical behaviour of loose sandy soils, particularly at small strain levels that are critical for seismic ground response and estimation of small ground deformation during construction. This study investigates the variation of small-strain shear properties of loose sand considering liquefaction histories. A series of laboratory experiments were conducted using cyclic triaxial tests combined with local small strain (LSS) and bender element measurements on Toyoura sand specimens prepared at a relative density (D_r) of 40% at depositional angles of 0°, 45°, and 90°. The results were compared with data for D_r = 60% obtained from a previous study, which was used to discuss the range of application using previous and current achievements. The results show that, before liquefaction, the initial shear modulus (G_0) increases with increasing depositional angle, indicating anisotropic soil behaviour. However, after liquefaction, G_0 becomes independent of depositional angle, indicating that the liquefaction process largely changes the soil structure. In addition, the degradation of secant shear modulus (G_{sec}) at Dr = 40% is more pronounced than at D_r = 60%, highlighting the greater susceptibility of loose sand to stiffness reduction under cyclic loading. To study the mechanism of soil liquefaction, the relationship between liquefaction resistance and small-strain shear properties was investigated. The results showed a strong correlation between liquefaction resistance (CRR) and shear modulus at very small strain levels (0.001% and 0.01%) for both D_r = 40% and D_r = 60%. This suggests that small-strain shear properties can provide a reliable indicator for assessing liquefaction resistance. However, G_{sec} at strain level greater than 0.01% showed the opposite trend with CRR. Overall, the effects of liquefaction history on mechanical properties were able to well explain using variation of particle orientation measured by optical microscopy. These findings contribute to more accurate prediction of ground liquefaction under seismic loading.

Keywords: Liquefaction, cyclic triaxial test, bender element, LSS, initial shear modulus, liquefaction resistance

1. INTRODUCTION

The deformation behavior of saturated sandy soils under cyclic loading is strongly influenced by the reduction in effective stress and shear strength during earthquakes. This phenomenon, commonly known as liquefaction, has become a major concern in geotechnical engineering because of its impact on the stability and performance of civil infrastructure (Seed and Idriss, 1971; Kramer, 1996). Although considerable research has focused on evaluating liquefaction resistance, the influence of liquefaction on the small-strain shear properties of loose sand remains less understood. These properties are closely related to the soil fabric and play an important role in evaluating the deformation behavior of geotechnical structures.

The initial shear modulus (G_0) and secant shear modulus (G_{sec}) are widely used to characterize soil stiffness at very small and medium strain levels, respectively (Hardin and Drnevich, 1972). Since liquefaction causes particle rearrangement and modifies the soil fabric, significant changes in stiffness characteristics can occur even after re-consolidation. In addition, depositional particle orientation influences the initial soil fabric and may affect stiffness degradation before and after liquefaction. However, studies investigating the combined effects of liquefaction history and particle orientation on the small-strain shear properties of loose sand remain limited.

Therefore, this study investigates the variation of the small-strain shear properties of loose Toyoura sand before and after liquefaction. Bender element (BE) and local small-strain (LSS) measurements were used to evaluate G_0 and G_{sec} over a strain range of approximately 0.0001% to 1%.

Furthermore, the effects of depositional angle and liquefaction history on stiffness degradation were investigated, and the relationships between liquefaction resistance (CRR), G_{sec}, and compressive strength at large strains (q_{max}) were examined to improve understanding of post-liquefaction deformation characteristics.

2. EXPERIMENTS

2.1 Testing material and specimen preparation

The soil for this study is a Toyoura sand, a soil standard used in Japan. This sand is collected from Yamaguchi beach (Yamaguchi prefecture, Japan). The particle size distribution indicates that Toyoura sand is a poorly graded fine quartz rich sand that is sub-angular to angular (Figure 1). The physical parameters of the sand are shown on table 1.

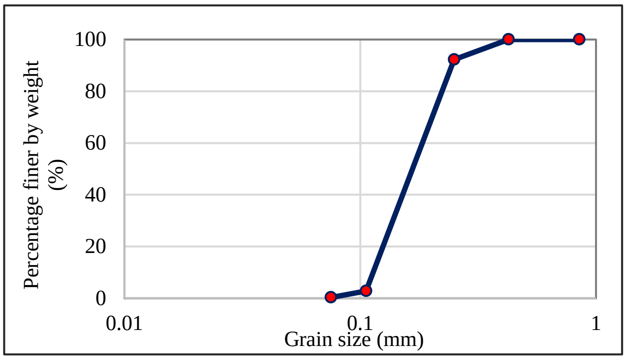

Fig. 1. Grain size distribution of Toyoura sand.

Table 1: Physical properties of Toyoura sand.

Specific gravity ρ (g/cm^3)	2.65
Max void ratio e_{max}	0.990
Min void ratio e_{max}	0.597
Uniformity coefficient U_c	1.48
Diameter at 50% D_{50} (mm)	0.2

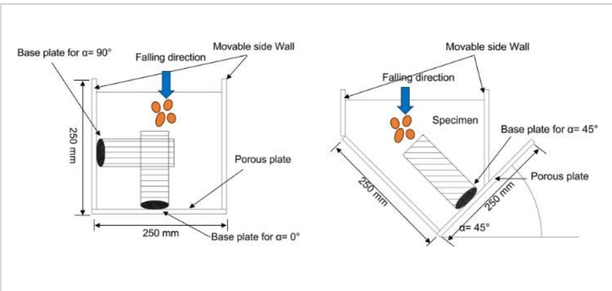

Fig. 2. Mold for specimen preparation at 0°, 45°, and 90°.

A rectangular container (250 mm height x 250 mm length x 100 mm width) consisting of six separated metal walls connected by fastening screws was designed and fabricated to prepare specimen. As illustrated in Fig. 2, two movable side walls were adjusted to achieve different depositional angles (α) of 0°, 45°, and 90°.

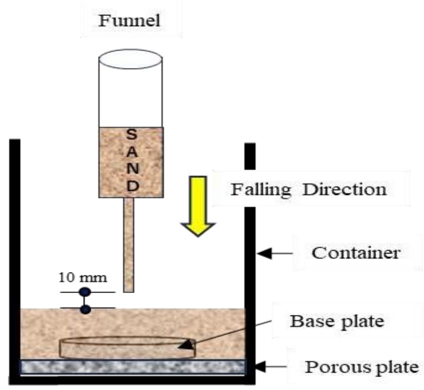

Fig. 3. Air Pluviation method.

As shown in Fig. 3, the sand was poured through a funnel into a container. The sand was poured at a constant falling height of 10 mm to achieve 40% relative density. The container filled with sand was then submerged in water to achieve saturation, after which the water was allowed to drain naturally. Residual water was subsequently removed by applying a vacuum pressure of -20 kPa. Following careful disassembly of the container's side walls, the sand block can remain self-supporting because of suction effects. A cylindrical specimen of 125 mm in height and 50 mm in diameter was trimmed from the sand block. Figure 4 presents sand block conditions after removal of side walls in α = 0°, 45°, and 90°.

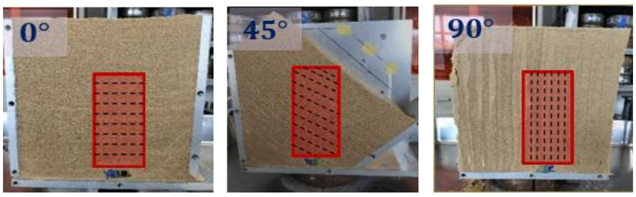

Fig. 4. Preparation of the specimen with different depositional angles α.

2.2 Testing apparatus

A triaxial apparatus equipped with local small-strain (LSS) and bender element (BE) measurement systems (Toyota et al. 2017) was used to investigate the deformation characteristics of sand (Fig. 5). Two metallic targets spaced 80 mm apart were attached to the specimen surface to measure the local axial strain (ε_a), while the radial strain (ε_r) was measured at the specimen mid-height using a proximity transducer. The G_{sec} was calculated from the measured deviator stress and shear strain, and the equations are as follows:

$$G_{\mathrm{sec}} = q/3\varepsilon_{\mathrm{s}} \qquad (1)$$

$$\varepsilon_{\mathrm{s}} = 2/3(\varepsilon_{\mathrm{a}} - \varepsilon_{\mathrm{r}}) \qquad (2)$$

$$q = \sigma'_{a} - \sigma'_{r} \qquad (3)$$

where q is the deviator stress, ε_{s} is shear strain, σ_{a}' and $\sigma_{\mathrm{r}}'$are axial effective stress and radial effective stress, respectively.

To determine the G_0, bender elements were installed in the top cap and pedestal as the transmitter and receiver, respectively. BE tests were conducted in accordance with the Japanese Geotechnical Society JGS (2011) standard using input frequencies of 15 kHz, 20 kHz, 25 kHz and 30 kHz. The shear wave propagation time was measured by the start-to-start method as shown in Figure 7. The distance of a wave (L_{tt}) was measured from the tip-to-tip of the transmitter and receiver elements, which is about 12 cm. Shear wave velocity (V_s) was obtained from the ratio of the distance travelled and the measured propagation time.

The G_0 was then obtained using the following relationship:

$$G_0 = \rho_{\mathrm{t}}.V_{\mathrm{s}}^2 = \rho_{\mathrm{t}}(\frac{L_{\mathrm{tt}}}{\Delta t})^2$$

where ρ is the mass density of the soil specimen and V_s is the shear wave velocity.

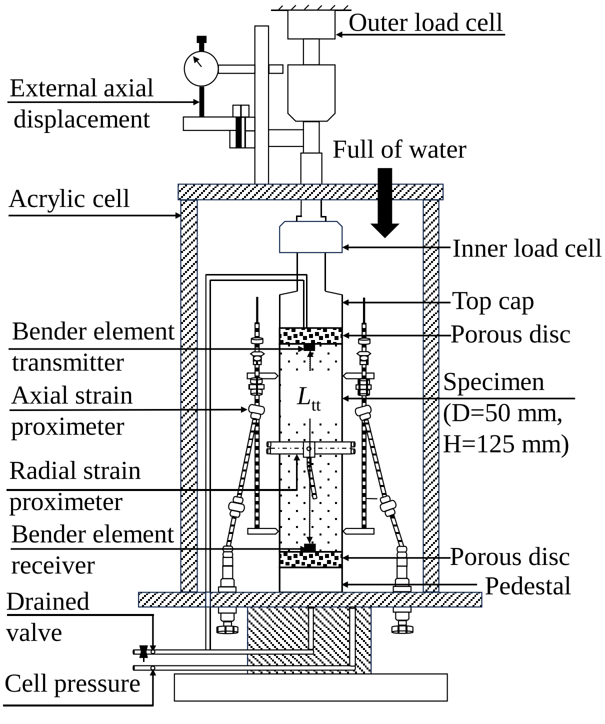

Fig. 5. Local small strain devices.

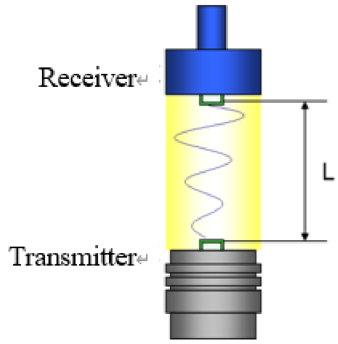

Fig.6 Bender element test.

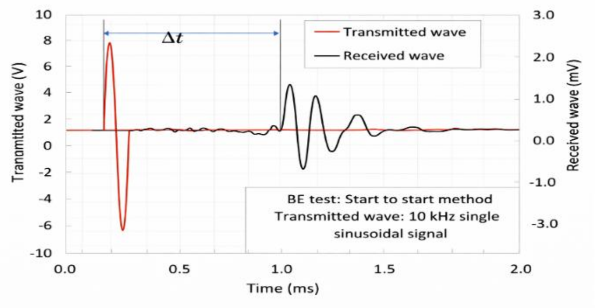

Fig. 7. Transmitted wave and received wave in BE test.

2.3 Testing procedures

The triaxial testing procedures consist of the following steps:

(1) Double negative pressure

To improve the saturation of the specimen, a double negative pressure technique was used. Vacuum pressures of approximately −100 kPa and −80 kPa were applied inside and outside the specimen, respectively, resulting in an effective stress of about 20 kPa. This method facilitated the removal of trapped and dissolved air from the soil pores and degassed the water before saturation, thereby improving the degree of saturation while maintaining specimen stability and preventing deformation during vacuum applications.

(2) Saturation process

After the double negative pressure treatment, degassed water was introduced from the bottom of the specimen to achieve full saturation (Rad and Clough, 1984). The applied negative pressures were gradually reduced to 0 kPa, while the cell pressure and pore water pressure were simultaneously increased to maintain an effective stress of approximately 20 kPa and ensure specimen stability. The specimen was then pre-consolidated, and saturation was verified using Skempton's B-value. A B-value of 0.95 or greater was considered to indicate full saturation before the subsequent testing stages.

Once the specimen was saturated, the local small strain (LSS) devices were installed to the specimen to measure the axial deformation at very small strain levels directly from the specimen's surface.

(3) Back pressure

The degree of saturation of the specimen was further increased by introducing back pressure after the installation of LSS device. This is important to remove the air left in the pores and provide complete saturation of the soil sample

(4) Isotropic consolidation process

The specimen was isotropically consolidated under an effective confining pressure of 50 kPa. After consolidation, bender element (BE) tests were conducted to determine the G_0 before liquefaction.

(5) Liquefaction process

Following consolidation and BE measurements, cyclic triaxial loading was applied with a deviator stress of 15 kPa (cyclic stress ratio, CSR = 0.15) at an axial strain rate of 0.5%/min. The test continued until the excess pore water pressure ratio (EPWPR) reached 95%, corresponding to an axial strain of approximately 1%, indicating the onset of liquefaction.

(6) Reconsolidation

After liquefaction, the specimen was then re-consolidated under an isotropic effective confining pressure of 50 kPa until the pore water pressure and volume change stabilized, after which bender element (BE) tests were performed to determine the G_0 after liquefaction.

(7) Shearing process

Monotonic compression tests were conducted under drained conditions at a constant confining pressure with an axial strain rate of 0.01%/min. The tests were performed on specimens before liquefaction and after re-consolidation to evaluate the influence of liquefaction on shear behavior. For specimens tested before liquefaction, the cyclic loading stage was omitted.

3 TESTING RESULTS AND DISCUSSIONS

3.1 Bender Element Test Results

The variation of the G_0 with depositional angle (α), obtained from the BE tests, is presented in Figure 8. The results presented are based on the present study carried out at D_r=40% compared with a previous study carried out at D_r=60% and both studies were conducted under an effective confining pressure of p'=50 kPa. The results display that before liquefaction; the G_0 increases as the α increases for both the relative densities. The values of G_0, however, are seen to be independent of the α after liquefaction for both the densities.

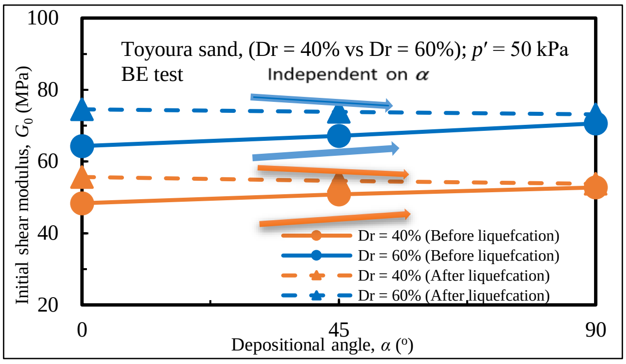

Fig. 8. Initial shear modulus of sand in BE tests for Dr=40% and Dr=60%.

3.2 Local Small Strain (LSS) Results

Figures 9 and 10 present the variation of the G_{sec} with shear strain (εs), together with the G_0 obtained from the BE tests, before and after liquefaction for loose Toyoura sand at Dr = 40% (present study).

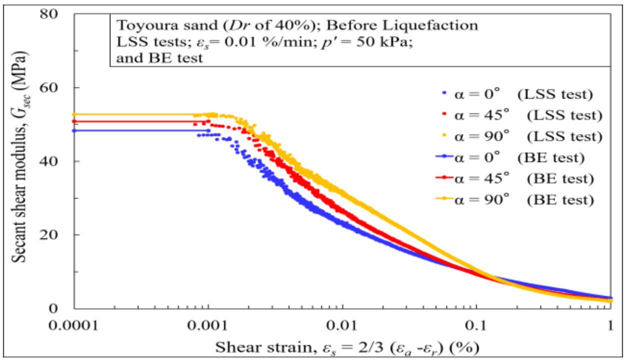

Fig. 9. Secant shear modulus of sand at Dr=40% (Before Liquefaction).

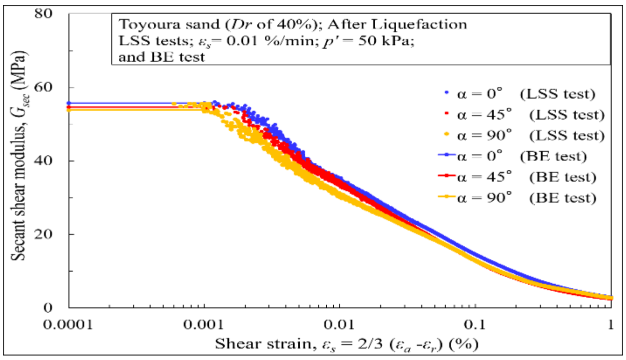

Fig. 10. Secant shear modulus of sand at Dr=40% (After Liquefaction).

For comparison, the corresponding results for Dr = 60% from the previous study are shown in Figures 11 and 12.

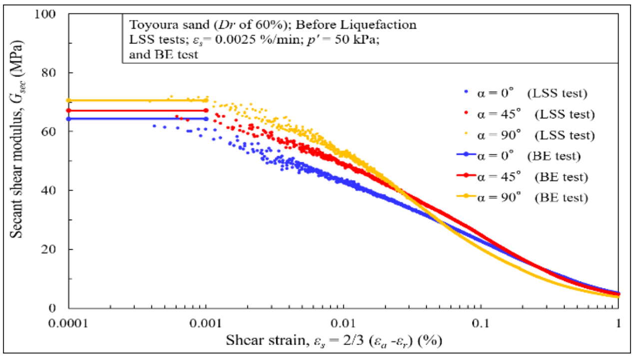

Fig. 11. Secant shear modulus of sand at Dr=60% (Before Liquefaction).

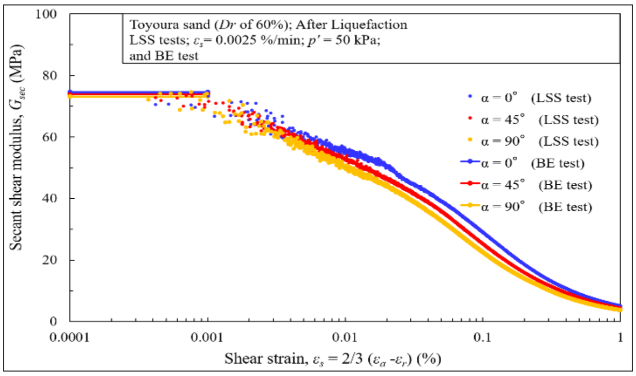

Fig. 12. Secant shear modulus of sand at Dr=60% (After Liquefaction).

Before liquefaction, the highest G_{sec} at very small strains (εs < 0.001%) was observed for the vertically deposited sand (α = 90°), whereas the lowest was obtained for the horizontally deposited sand (α = 0°). As the shear strain increased, this trend reversed, with α = 0° exhibiting the highest G_{sec}. After liquefaction, G_{sec} at very small strains became nearly independent of the depositional angle, indicating that the initial soil fabric was largely destroyed by liquefaction. At larger strain levels, however, the horizontally deposited sand exhibited slightly higher G_{sec} than the vertically deposited sand, suggesting that a small degree of the initial fabric remained after liquefaction. The same overall trends were observed for both relative densities, although stiffness degradation was more pronounced for Dr = 40% than for Dr = 60%.

3.3 Monotonic Compression Test Result

As discussed in the LSS results, the trend observed at very small strains changes as the strain increases. While the 90° depositional angle exhibited higher stiffness at small strains, this trend is reversed at larger strains.

Figures 13 and 14 present the monotonic compression test results before and after liquefaction for loose Toyoura sand, whereas figures 15 and 16 show the corresponding results for Dr = 60% (previous study), Before liquefaction, the specimen with a depositional angle of 0°developed the highest peak deviator stress (q_{max}) for both relative densities. After liquefaction, however, the compressive strength became nearly independent of the depositional angle, indicating that the initial soil fabric was largely disturbed by liquefaction.

These results suggest that although the 90°specimen is initially stiffer, the 0° specimen mobilizes greater particle interlocking and shear strength during large-strain deformation.

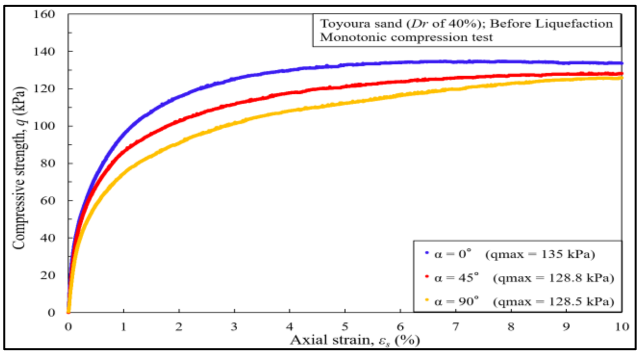

Fig. 13. Variation of $q_{\max}$ before liquefaction (Dr = 40%).

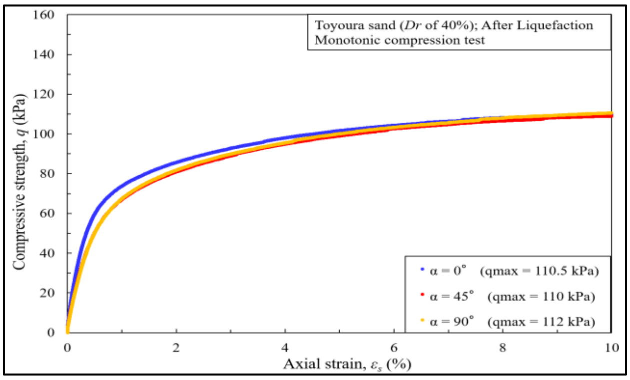

Fig. 14. Variation of $q_{\max}$ after liquefaction (Dr = 40%).

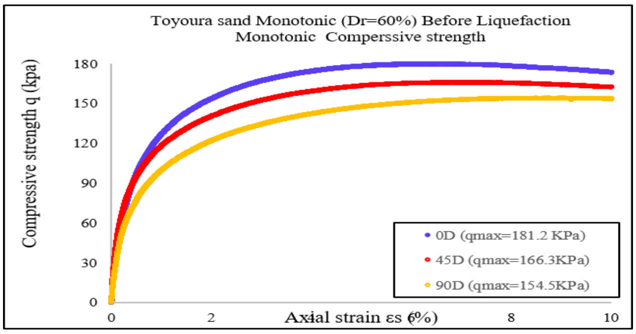

Fig. 15. Variation of $q_{\max}$ before liquefaction (Dr = 60%).

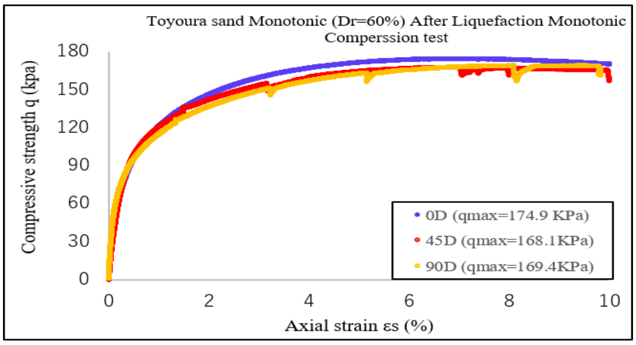

Fig. 16. Variation of $q_{\max}$ after liquefaction (Dr = 60%).

3.4 Correlation of Liquefaction Resistance with Secant Shear Modulus (G_{sec}) and q_{max}.

Figure 17 shows the relationship between CRR and the G_{sec} at different shear strain levels. At very small strains (0.001%–0.01%), a positive correlation is observed, indicating that specimens with higher small-strain stiffness exhibit greater liquefaction resistance. However, as the shear strain increases to 0.1% and 1%, the correlation reverses. This change suggests that the influence of the initial small-strain stiffness gradually diminishes, and the soil behavior becomes governed by stiffness degradation and large-strain deformation.

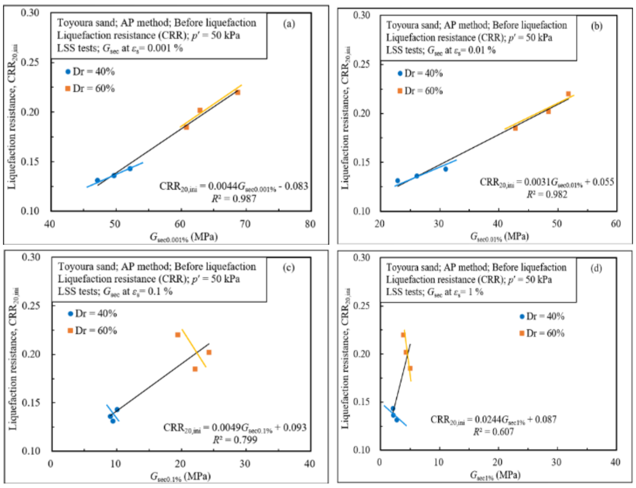

Fig 17. Relationship between CRR and G_{sec} at small different strain levels for both Dr = 40% and Dr = 60%.

To examine whether this trend persists at larger strain levels, the relationship between CRR and the peak compressive strength (q_{max}) obtained from the monotonic compression tests was investigated, as shown in Figure 18. The results demonstrate that the reversed correlation continues at large strains, indicating that specimens exhibiting higher compressive strength tend to have lower liquefaction resistance.

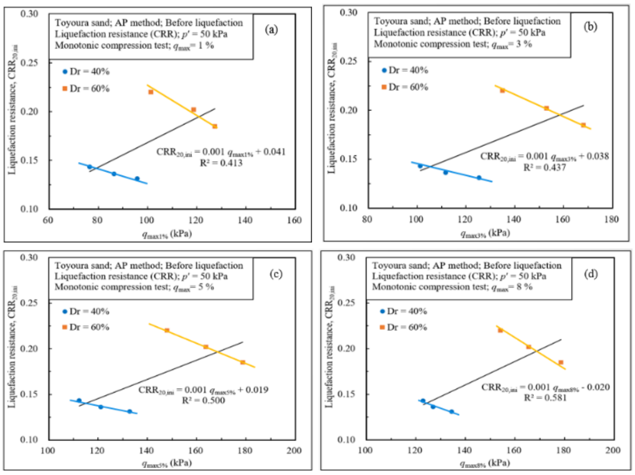

Fig 18. Relationship between CRR and q_{max} at different large strain levels for both Dr = 40% and Dr = 60%.

4 Conclusions

This study investigates the influence of liquefaction on the small-strain shear parameters of loose Toyoura sand. Based on the experimental results, the following conclusions can be drawn:

1. Before liquefaction, the G_0 increased with increasing depositional angle. This indicates that the initial soil fabric and particle arrangement produced anisotropic stiffness behavior.
2. After liquefaction, G_0 and G_{sec} became nearly independent of depositional angle; liquefaction history diminishes deposition-induced anisotropy.
3. G_{sec} at ε_s = 0.001% to 0.01% exhibits strong correlation with *CRR*; including both depositional angle and density effects.
4. At small strains, the vertically deposited specimen (α = 90°) exhibited the highest G_{sec}, whereas at larger strains the trend reversed, with the horizontally deposited specimen (α = 0°) showing the highest G_{sec}.

ACKNOWLEDGEMENTS

I would like to express my sincere gratitude to my supervisor, Professor Hirofumi Toyota, for his invaluable guidance throughout this research. I also thank my seniors, colleagues, and everyone who contributed to the successful completion of this study.

REFERENCES

1) Hardin, B. O., and Drnevich, V. P. (1972): Shear modulus and damping in soils: measurement and parameter effects. Soil Mechanics and Foundations Division, ASCE, 98(SM6), 603-624
2) Japanese Geotechnical Society. (2011): JGS 0544:

Method for laboratory measurement of shear wave velocity of soils by bender element test. Tokyo: Japanese Geotechnical Society.
3) Kramer, S. L. (1996): Geotechnical earthquake engineering. Prentice Hall. https://doi.org/10.1007/978-3-319-61648-3_5.
4) Le, N. B., Toyota, H. and Takada, S. (2020): Evaluation of mechanical properties of mica-mixed sand considering inherent anisotropy. Soils and Foundations, 60(2), 533–550.
5) Seed, H. B., and Idriss, I. M. (1971): Simplified procedure for evaluating soil liquefaction potential. Journal of the Soil Mechanics and Foundations Division, 97(SM9), 1249-1273.
6) Skempton, A. W. (1954): The pore-pressure coefficients A and B. Géotechnique, 4(4), 143-147.
7) Toyota, H., and Takada, S. (2016). Variation of liquefaction strength is induced by monotonic and cyclic loading histories. Journal of Geotechnical and Geoenvironmental Engineering, 143(2), 04016120
8) Toyota, H., and Takada, S. (2017): Variation of Liquefaction Strength Induced by Monotonic and Cyclic Loading Histories. Journal of Geotechnical and Geoenvironmental Engineering, 143(4), 04016120